NASA-TM-83011

NASA Technical Memorandum 83011

NASA-TM-83011 19830004088

Numerical Simulation of the Flow and Fuel-Air Mixing in an Axisymmetric Piston-Cylinder Arrangement

Tom I-P. Shih
Lewis Research Center
Cleveland, Ohio

and

Gene E. Smith and George S. Springer
The University of Michigan
Ann Arbor, Michigan

October 1982

NASA

UTTL: Numerical simulation of the flow and fuel-air mixing in an axisymmetric piston-cylinder arrangement

AUTH: A/SHIH, T. I. P.; B/SMITH, G. E.; C/SPRINGER, G. S.   PAA: B/(Michigan Univ, Ann Arbor); C/(Michigan Univ., Ann Arbor)
CORP: National Aeronautics and Space Administration. Lewis Research Center, Cleveland, Ohio.   AVAIL.NTIS   SAP: HC A02/MF A01
MAJS: /*ASYMMETRY/*COMPUTERIZED SIMULATION/*FLUID MECHANICS/*FUEL-AIR RATIO/*GAS PRESSURE/*INTERNAL COMBUSTION ENGINES/*LAMINAR FLOW/*PISTONS
MINS: / COMPRESSION TESTS/ FLOW DISTRIBUTION/ GAS MIXTURES/ TRANSPORT PROPERTIES / VORTICES
ABA: Author

ABS: The implicit factored method of Beam and Warming was employed to describe the flow and the fuel-air mixing in an axisymmetric piston-cylinder configuration during the intake and compression strokes. The governing equations were established on the basis of laminar flow. The increased mixing due to turbulence was simulated by appropriately chosen effective transport properties. Calculations were performed for single-component gases and for two-component gases and for two-component gas mixtures. The flow field was calculated as functions of time and position for different geometries, piston speeds, intake-charge-to-residual-gas-pressure ratios,

ENTER: PAGE

and species mass fractions of the intake charge. Results are presented in graphical form which show the formation, growth, and break-up of those vortices which form during the intake stroke and the mixing of fuel and air throughout the intake and compression strokes. It is shown that at bore-to-stroke ratio of less than unity, the vortices may break-up during the intake stroke. It is also shown that vortices which do not break-up during the intake stroke coalesce during the compression stroke. The results generated were compared to existing numerical solutions and to available experimental data.

NUMERICAL SIMULATION OF THE FLOW AND FUEL-AIR MIXING IN

AN AXISYMMETRIC PISTON-CYLINDER ARRANGEMENT

by

Tom I-P. Shih
National Aeronautics and Space Administration
Lewis Research Center
Cleveland, Ohio

and

Gene E. Smith and George S. Springer
The University of Michigan
Ann Arbor, Michigan

ABSTRACT

The implicit factored method of Beam and Warming was employed to describe the flow and the fuel-air mixing in an axisymmetric piston-cylinder configuration during the intake and compression strokes. The governing equations were established on the basis of laminar flow. The increased mixing due to turbulence was simulated by appropriately chosen effective transport properties. Calculations were performed for single-component gases and for two-component gas mixtures. The flow field was calculated as functions of time and position for different geometries, piston speeds, intake-charge-to-residual-gas-pressure ratios, and specie mass fractions of the intake charge. Results are presented in graphical form which show the formation, growth, and break-up of those vortices which form during the intake stroke and the mixing of fuel and air throughout the intake and compression strokes. It is shown that at bore-to-stroke ratio of less than unity, the vortices may break-up during the intake stroke. It is also shown that vortices which do not break-up during the intake stroke coalesce during the compression stroke. The results generated were compared to existing numerical solutions and to available experimental data.

I. INTRODUCTION

An understanding of the flow patterns inside cylinders of spark ignited reciprocating engines is required in developing efficient, low emission engines. For this reason, numerous investigators have studied flows inside the cylinders of reciprocating engines by both experimental (e.g., see survey in ref. 1) and numerical (e.g., see surveys in refs. 1 to 4) techniques. However, owing to the complexity of the phenomena, a complete description of the flow cannot be obtained by presently available experimental and numerical methods. Instead, progress towards the solution must be made by focusing attention on certain aspects of the problem. In this study, the flow patterns and mixture distributions were investigated inside an axisymmetric piston-cylinder configuration during the intake and compression strokes. The results were generated by a numerical method of solution of the governing equations.

II. DESCRIPTION OF THE PROBLEM

The following problem was analyzed. A hollow circular cylinder (inner radius r_p) is closed on one end by a flat piston and on the other end by a flat plate (fig. 1). The piston is connected to a crank shaft (radius r_c) through a connecting rod (length l_c). The piston is driven by rotation of the crank shaft about the crank pin at an angular velocity of Ω, resulting in a piston velocity of u_p.

The flat plate has a centrally located annular opening (valve opening, inner radius r_v, outer radius r_H) in it which opens instantaneously at the beginning of the intake stroke (crank angle $\phi = 0$) and closes instantaneously at the end of the intake stroke ($\phi = \pi$).

The temperatures at the cylinder wall T_w, valve T_v, cylinder head T_h, and piston T_p are constants, but may have different values.

The fluid enters the piston-cylinder configuration described above (henceforth referred to as the cylinder) through the valve opening during the intake stroke. The static temperature T_i and static pressure P_i of the entering fluid are both constant. At the valve opening (seat angle α), the entering fluid may have velocity components in the radial (V_r) and axial (V_z) directions, but not in the tangential direction. The magnitude of the velocity at the valve opening depends upon the instantaneous flow field inside the cylinder as well as the static temperature and pressure of the fluid at the valve opening.

The viscous and thermally conducting fluid which enters the cylinder (intake charge) is either a single-component ideal gas or a two-component nonreacting ideal gas mixture. The two-components of the intake charge are to simulate air and fuel. The thermodynamic and transport properties of the intake charge (except for the binary diffusion coefficient) are taken to be constants. The binary diffusion coefficient between the two-components, D_{AB}, is taken to be inversely proportional to the local mixture density ρ. The mass fraction of the two-component ideal gas mixture (X_A and X_B) may vary arbitrarily with time at the valve opening.

At the beginning of the intake stroke, the gas in the clearance volume (residual gas) is taken to be a stagnant, single-component ideal gas at static temperature T_i and static pressure P_c ($P_c \leq P_i$). The residual gas has the same thermodynamic and transport properties as component A of the intake charge.

The problem just described is symmetric with respect to the axis of the cylinder. Accordingly, the tangential velocity is zero everywhere in the cylinder, and the radial velocity and the first-order radial derivatives of density, mass fractions of components A and B, axial velocity, and energy are zero at the center line.

III. METHOD OF SOLUTION

The basic equations governing the problem are the conservation equations of mass, radial momentum, axial momentum, and energy and the specie balance equations (refs. 5 and 6). To render these equations more amenable to numerical methods of solution, the following simplifications were made: (a) pressure gradient contribution to specie diffusion and momentum transport due to specie diffusion were not considered; (b) irreversible coupling effects between the temperature gradient and specie concentration gradient (Soret and

Dufour effects) were neglected; (c) body forces were neglected; (d) the bulk viscosity was taken to be zero; and (e) radiation heat transfer was neglected.

The governing equations, applicable to laminar flows, are summarized in table 1. The increased mixing due to turbulence was simulated by appropriately chosen effective transport properties (Section IV). Equations (1) to (19) constitute a closed system in the five basic dependent variables: density (ρ), mass fraction of component A (X_A), radial velocity (V_r), axial velocity (V_z), and energy (e).

The boundary and initial conditions corresponding to equations (1) to (19) are given in table 2. The no-slip condition requires the fluid velocity next to a solid wall to be equal to the velocity of the solid wall (eqs. (20) and (21)).

The gas temperature next to solid walls equals the temperature of the walls. With all walls maintained at constant temperatures, this boundary condition results in equations (22) to (25).

The cylinder walls are assumed to be nonporous. This boundary condition is expressed by equations (26) and (27). The static pressure and static temperature of the gas at the valve opening are constant with respect to time as reflected by equation (28). The mass fraction of component A at the valve opening is expressed by equation (29). The radial and axial velocities at the valve opening are related, as indicated by equation (31). The axial velocity at the valve opening is determined by applying the conservation of mass equation at the valve opening (eq. (32)).

Furthermore, the symmetry conditions at the center line result in equation (33). At time t equal to zero, the piston is at the TDC position ($\phi = 0$) and the residual gas in the clearance volume is a stagnant single-component ideal gas at static pressure P_c and static temperature T_i. These initial conditions are specified by equation (34).

Solutions to the governing equations and the corresponding initial and boundary conditions formulated above must be obtained by numerical methods. In this investigation, the implicit-factored, finite-difference method of Beam and Warming (refs. 7 and 8) was used to obtain solutions. The detailed steps of the method was described elsewhere (refs. 9 and 10) and will not be repeated here. Essentially, the continuous domain inside the cylinder was represented by a grid system. The grid size in the axial direction was uniform but changed with time as the piston moved towards or away from the cylinder head. The grid spacing in the radial direction did not change with time, but varied in size to resolve regions where the radial derivatives were steep. The governing equations were first transformed to a moving coordinate system corresponding to this grid and were then expressed in finite-difference form. The resulting system of finite-difference equations had block tridiagonal coefficient matrices and hence could be solved by the Thomas algorithm (refs. 11 and 12). In addition, the boundary conditions were expressed in a form consistent with the implicit factored method of Beam and Warming and the Thomas algorithm. A complete description of the equations may be found in reference 9. A copy of the computer code may be obtained from the authors.

IV. RESULTS

Numerical solutions were obtained to explore the flow patterns and the mixture distributions inside the cylinder during the intake and compression

strokes. Two types of problems were studied: (a) single-component gas flows, and (b) two-component gas mixture flows.

The ranges of the parameters for which numerical solutions were obtained are summarized in table 3. The values of the parameters describing the geometry and operating conditions were selected so as to correspond to those typically found in spark-ignition engines. In selecting thermodynamic and transport properties, two constraints were taken into account. First, the values were selected so as to be physically reasonable, as will be discussed subsequently. Second, the values were chosen so as to permit the use of convenient grid sizes (ref. 9).

For problems involving a single-component gas, the thermodynamic properties of the gas were those of air at temperature T_i. For problems involving a two-component gas mixture, the thermodynamic properties were those of air at temperature T_i for component A, and those of octane at temperature T_i for component B. In every problem, T_i was the temperature of the intake charge and the initial temperature of the residual gas.

The value of the viscosity, μ, was based on the observation that the effective viscosity for turbulent flows inside spark ignition engine cylinders is roughly 100 times higher than the viscosity corresponding to laminar flows (ref. 13). The laminar viscosity of air at temperature T_i (340 K) and atmospheric pressure is 3.203×10^{-5} kg/m-s. The value of the effective viscosity used is 100 times this value (table 3).

The values of the mass diffusivity, D_{AB}, and thermal conductivity, λ, were selected by taking the turbulent Schmidt, Sc, and Prandtl, Pr, numbers to be equal to unity (refs. 14 and 15)

$$Sc = \frac{\mu}{\rho D_{AB}} = 1 \qquad\qquad Pr = \frac{\mu C_p}{\lambda} = 1 \qquad\qquad (35)$$

One set of calculations were performed in which the effective transport properties (μ and λ) were reduced by a factor of 100. The results obtained with the different transport properties (but with the same geometric and operating conditions) showed the flow patterns for the two problems to be almost identical.

The axial and radial components of the gas velocities inside the cylinder were calculated as functions of time and represented graphically. Only the graphical results were presented here. The resultant velocities are represented by arrows, drawn to scale when the magnitude of the velocity vectors are less than or equal to 0.5 meter per second. When the magnitude of the velocity vector is greater than 0.5 meter per second, it is set equal to 0.5 meter per second.

Single Component Gas - Intake Stroke

The results are shown in figures 2 to 6. Throughout the intake stroke, a jet issued from the valve opening. For the conditions employed in this study, the jet always impinged on the piston surface (figs. 2 to 6). The existence of such a jet has been observed previously in both experimental (refs. 16 to 22) and numerical (refs. 23 to 38) studies of similar piston-cylinder problems.

During the first part of the intake stroke (crank angle ϕ less than ~10 degrees measured from the TDC position), only the jet existed inside the cylinder and there were no recirculating flows. The reason for this is that the pressure across the valve opening was taken to be constant. This allowed the jet to spread out radially from the valve opening without causing the jet

to separate. In an actual piston-cylinder, where the static pressure across the valve opening would not be constant, recirculating flows may be established earlier than is accounted for in this study.

At some crank angles greater than ~10 degrees (but always less than 90 degrees), flow separation produced two recirculating flows having the shape of toroidal vortices. One of these vortices (referred to as the cylinder-head vortex) was located between the jet and the cylinder wall. The other (referred to as valve vortex) was located between the jet and the center line. The formation of such vortices during the intake stroke has been observed previously both in experimental (refs. 17 to 22) and numerical (refs. 23 to 39) studies.

The formation and subsequent behavior of these vortices depended largely on the speed and angle of the jet issuing from the valve opening. The jet speed is a function of the pressure difference across the valve opening (i.e., the difference between the constant pressure of the intake charge P_i and the instantaneous pressure of the gas inside the cylinder). On one hand, the pressure inside the cylinder increases with time due to the influx of the gas. On the other, the pressure inside the cylinder decreases with time due to the motion of the piston away from the cylinder head.

When the intake charge pressure was the same as the residual gas pressure ($P_i/P_c = 1$), the jet speed continuously increased as the piston moved away from the cylinder head until the crank angle ϕ reached 90 degrees. Thus, once the cylinder-head and valve vortices were formed, the jet continuously strengthened these vortices, and the vortices steadily grew in size throughout the intake stroke. The growth of the vortices during the intake stroke was observed previously in experimental (refs. 17 to 21) and numerical (refs. 26 to 38) studies.

Previously, Ekchian and Hoult (ref. 17) reported the speed with which the cylinder-head and valve vortices moved. These investigators performed experiments with a valve-seat angle of 45 degrees, a piston-to-valve opening area ratio of 23.5, bore-to-stroke ratios of 0.75 to 1.35, and crankshaft angular speeds of 750 to 2500 rpm. Ekchian and Hoult noted that: (a) the valve vortex grew in size and its center of rotation moved at about one-half of the piston speed during the intake stroke; (b) the cylinder-head vortex was approximately constant in size and was almost stationary during the intake stroke; and (c) the cylinder-head vortex was trapped in the volume formed by the jet, the cylinder head, and the cylinder wall.

Ekchian and Hoult's results can be compared with the numerical calculations performed here for valve seat angle α equal to 45 degrees, piston-to-valve-opening area ratio of 4, bore-to-stroke ratio of 1.67, and crank-shaft angular speed of 400 rpm. These numerical results show the following phenomena: (a) the valve vortex grew in size and its center of rotation moved at about one-third to one-half of the piston speed as the piston moved away from the cylinder head (fig. 2). This is in fair agreement with the experimental observations of Ekchian and Hoult (ref. 17), and (b) the cylinder-head vortex grew in size and its center of rotation moved at about one-fifth of the piston speed (fig. 2).

The growth of the cylinder-head vortex and its corresponding motion resulted from the fact that the jet bent towards the piston. This bending increased the volume available for the vortex to occupy. In Ekchian and Hoult's experiment, the jet remained straight; hence the size of the cylinder-head vortex remained constant and its center of rotation did not move. The reason that the jet did not bend in their experiment is probably due to the fact that the jet speed in their experiment was higher than the jet speed simulated in this study.

5

When the intake charge pressure is higher than the residual gas pressure $(P_i/P_c > 1)$, then, depending of the piston speed, the speed of the jet may first increase, then decrease, and then increase again. During the first jet-speed increase, both the cylinder-head and valve vortices formed. Depending on the jet speed and the strength of the cylinder-head and valve vortices formed during the first jet-speed increase, these vortices may diminish in strength or even completely die out during the subsequent decrease in jet speed. When the vortices die out, a new set of cylinder-head and valve vortices form when the jet speed increases again due to the piston motion (fig. 3). It is interesting to note that the flow patterns inside the cylinder formed with the intake-charge-to-residual-gas pressure ratios of unity and 1.036 become similar at crank angles beyond ~40 degrees (figs. 3 and 4).

The cylinder-head and valve vortices formed at different times. At higher piston speeds (and corresponding higher jet speeds), both the cylinder-head and valve vortices formed earlier. When the valve-seat angle α equals zero degrees, the cylinder-head vortex always formed before the valve vortex (figs. 4 to 6). When the valve-seat angle α equals 45 degrees, the valve vortex formed before the cylinder-head vortex (fig. 2).

The relative strengths of the cylinder-head and valve vortices depended upon the relative times at which these vortices form. When the valve vortex formed at crank angles near 90 degrees (i.e., at the point at which the jet speed began to decrease due to decreasing piston speed), the cylinder-head vortex was always stronger than the valve vortex (figs. 3 and 4). When the valve vortex formed early (ϕ = 30 to 60 degrees), the valve vortex became stronger than the cylinder-head vortex by the end of the intake stroke (figs. 2, 5, and 6).

At a low piston speed (Ω = 400 rpm and r_c = 0.03 meter) a third recirculating flow, in the shape of a toroidal vortex, formed between the valve vortex and the valve surface (fig. 4). Such a vortex was observed previously at low piston speeds both in experimental (refs. 19 and 21) and in numerical (refs. 37 and 38) studies.

At 400 rpm, bore-to-stroke ratio of 0.78, and valve-seat angle of zero degrees, the cylinder-head vortex broke up into two smaller toroidal vortices enclosed by a larger toroidal vortex (fig. 6). Ekchian and Hoult (ref. 17) observed the break-up of the valve vortex into a random flow. In the present study, the vortex did not degenerate into a random flow because instability and three-dimensional flow (needed for the complete vortex break-up) were not included in the numerical solution.

Single Component Gas – Compression Stroke

During the compression stroke, the cylinder-head and valve vortices were no longer separated by the jet, allowing the two vortices to interact (figs. 7 to 10). Because of the rotational motion of the two vortices, they forced each other towards the piston. Since the two vortices were of unequal strength, the weaker one was pushed closer to the piston surface by the stronger one.

As the piston speed increased during the compression stroke (crank angle ϕ between ~190 and 240 degrees), the two vortices began to coalesce. Coalesce as used here means combine by entrainment. The time of this coalescing depended upon the strength of the vortex which was nearer to the piston surface.

At crank angles ϕ between ~230 and 240 degrees, the two vortices coalesced into a single toroidal vortex. The coalescing of the cylinder-head and valve vortices has not been described by previous investigators. However, the disappearance of one vortex was found by Ashurst (ref. 26) and by Diwaker, et al. (ref. 27) in numerical simulations of similar piston-cylinder problems.

Towards the end of the compression stroke (crank angle $\phi > 320$ degrees) a new recirculating flow (corner vortex) formed in the corner of the cylinder head and cylinder wall. The numerical simulations of Chong, et al. (ref. 40) and Gosman, et al. (ref. 37) also showed the formation of the corner vortex. Both this study and Chong, et al. (ref. 40) indicate that the corner vortex formed earlier at lower piston speeds.

In an actual cylinder, a new vortex forms near the cylinder wall due to the piston scraping off the boundary layer next to the cylinder wall during the compression stroke (refs. 1 and 41 to 46). This vortex was not observed in the present study. One reason for this is that a large number of grid points would be required for a high enough resolution to observe this phenomenon.

Two-Component Gas Mixture

Numerical solutions were also obtained when the intake charge is a two-component gas mixture of components A and B. The mass fractions of components A and B at the valve opening varied with time according to the expression given in table 2. The mass fraction are represented graphically by symbols selected to give reasonable visual contrast for the different mass fractions inside the cylinder. The darker and lighter regions represent regions of lower and higher X_A, respectively.

Whether the intake charge was a single-component gas or a two-component gas mixture, the flow pattern inside the cylinder depended largely on the speed of the jet issuing from the valve opening during the intake stroke. In single-component gas problems, the density of the intake charge was constant and the jet speed depended only on the pressure difference across the valve opening. In two-component gas mixture problems, the intake charge density varied with time so that the jet speed depended not only on the pressure difference across the valve opening but also on the intake charge density.

As in single-component gas problems, a cylinder-head and a valve vortex formed. Since the jet speed varied with time during the intake stroke (as it did in single-component gas problems), the vortices formed during the early part of the intake stroke may weaken and then strengthen again, or may die out completely and then form again (fig. 11). During the latter part of the intake stroke and during all of the compression stroke, the essential features of the flow were similar for single-component and two-component gas mixtures (fig. 12).

At the beginning of the intake stroke, the gas inside the cylinder (the residual gas) was a single-component gas with the same properties as component A of the intake charge. As the intake charge (composed of components A and B) entered into the cylinder, mixing of the gases took place. As time progressed, the composition of the gas mixture inside the cylinder tended to become more uniform due to mass diffusion and convective flow. The degree of mixing depended on the spatial gradient of the mass fraction of component A, the speed with which the gas was convected to the various regions inside the

cylinder, and the time available for mass diffusion and convective flow. These parameters in turn depended on the geometry, the crankshaft angular speed, the intake-charge-to-residual-gas pressure ratio, and the mass fraction of component A at the valve opening (i.e., the nonhomogeneity of the intake charge). For the conditions employed in this study, the gas mixture inside the cylinder always became "homogeneous" before the end of the compression stroke (figs. 13 and 14). By "homogeneous," it is meant that the mass fraction of component A inside the cylinder was uniform to within plus or minus of one percent.

CONCLUDING REMARKS

The results generated in this study illustrate some of the major features of the flow inside an axisymmetric piston-cylinder configuration. The results were obtained by equations formulated for axisymmetric, laminar flows. From the results obtained thus far, it appears that it would be worthwhile to extend the implicit-factored method to the study of turbulent flows. Extension of the method to three-dimensional internal flows also appears worth exploring. Application of this method to three-dimensional piston-cylinder problems could shed light on the three-dimensional hydrodynamic instabilities and on the vortex break-up.

REFERENCES

1. Witze, P. O., ed.: Comparisons Between Measurement and Analysis of Fluid Motion in Internal Combustion Engines. SAND 81-8242, Sandia National Laboratories, Livermore, CA, Oct. 1981.

2. Boni, A. A.: Numerical Simulation of Flame Propagation in Internal Combustion Engines: A Status Report. SAE Paper No. 780316, 1978.

3. Mattavi, J. N.; and Amann, C. A., eds.: Combustion Modeling in Reciprocating Engines. Plenum Press, 1980.

4. Butler, T. D.; et al.: Multidimensional Numerical Simulation of Reactive Flow in Internal Combustion Engines. Progress in Energy and Combustion Sciences, Vol. 7, N. A. Chigier, ed., Pergamon Press, 1981, pp. 293-315.

5. Bird, R. B.; Stewart, W. E.; and Lightfoot, E. N.: Transport Phenomena. John Wiley and Sons, Inc., 1960.

6. Williams, F. A.: Combustion Theory. Addison-Wesley Publishing Co., 1965.

7. Warming, R. F.; and Beam, R. M.: On the Construction and Application of Implicit Factored Schemes for Conservation Laws. Symposium on Computational Fluid Dynamics, H. B. Keller, ed., American Mathematical Society, 1978, pp. 85-129.

8. Beam, R. M.; and Warming, R. F.: An Implicit Factored Scheme for the Compressible Navier-Stokes Equations. AIAA J., vol. 16, no. 4, Apr. 1978, pp. 393-402.

9. Shih, T. I-P.: Application of the Implicit Factored Method to Complex Flow Problems. Ph.D. Thesis, Department of Mechanical Engineering and Applied Mechanics, The University of Michigan, 1981.

10. Shih, T. I-P., Smith, G. E., Springer, G. S., and Rimon, Y., "Boundary Conditions for the Solution of Compressible Navier-Stokes Equations by the Implicit Factored Method," Journal of Computational Physics (submitted).

11. Isaacson, E.; and Keller, H. B.: Analysis of Numerical Methods. John Wiley and Sons, Inc., 1966, pp. 55-61.

12. Richtmyer, R. D.; and Morton, K. W.: Difference Methods for Initial-Value Problems, Second Ed., John Wiley and Sons, Inc., 1967, pp. 198-201.

13. Johnston, S. C.; et al.: Application of Laser Diagnostics to an Injected Engine. SAE Paper No. 790092, 1979.

14. Launder, B. E.; and Spalding, D. B.: Lectures in Mathematical Models of Turbulence. Academic Press, 1972, pp. 46-70.

15. Reynolds, A. J.: The Prediction of Turbulent Prandtl and Schmidt Numbers. Int. J. Heat Mass Transfer, vol. 18, no. 9, Sept. 18, 1975, pp. 1055-1069.

16. Semenov, E. S.: Studies of Turbulent Gas Flow in Piston Engines. Combustion in Turbulent Flow, L. N. Khitrin, ed., NASA TTF-97, 1963, pp. 122-147.

17. Ekchian, A.; and Hoult, D. P.: Flow Visualization Study of the Intake Process of an Internal Combustion Engine. SAE Paper No. 790095, 1979.

18. Gany, A.; Larrea, J.-J.; and Sirignano, W. A.: Laser-Doppler Velocimetry Measurements in a Motored I.C. Engine Simulator. AIAA Paper No. 80-0079, 1980.

19. Ramos, J. I.; Gany, A.; and Sirignano, W. A.: The Recirculating Flow Field in a Two-Stroke, Motored Engine: Comparison Between Theory and Experiments. Momemtum and Heat Transfer Processes in Recirculating Flows, HTD-Vol. 13, ASME, 1980, pp. 63-69.

20. Ramos, J. I.; Gany, A.; and Sirignano, W. A.: Study of Turbulence in a Motored Four-Stroke Internal Combustion Engine. AIAA J., vol. 19, no. 5, May 1981, pp. 595-600.

21. Morse, A. P.; Whitelaw, J. H.; and Yianneskis, M.: Turbulent Flow Measurements by Laser-Doppler Anemometry in Motored Piston-Cylinder Assemblies. J. Fluids Eng., vol. 101, no. 2, June 1979, pp. 208-217.

22. Namazian, M.; et al.: Schlieren Visualization of the Flow and Density Fields in the Cylinder of a Spark-Ignition Engine. SAE Paper No. 800044, 1980.

23. Sod, G. A.: Automotive Engine Modeling With a Hybrid Random Choice Method. SAE Paper No. 790242, 1979.

24. Sod, G. A.: A Hybrid Random Choice Method With Application to Internal Combustion Engines II. LBL-9423, Lawrence Berkeley Laboratory, University of California, 1979.

25. Sod, G. A.: Automotive Engine Modeling With a Hybrid Random Choice Method, II. SAE Paper No. 800288, 1980.

26. Ashurst, W. T.: Vortex Dynamic Calculation of Fluid Motion in a Four Stroke Piston 'Cylinder'-Planar and Axisymmetric Geometry. SAND 78-8229, Sandia Laboratories, 1978.

27. Diwaker, R.; et al.: Inviscid Solutions to the Flowfield in an Internal Combustion Engine. AIAA J., vol. 14, no. 12, Dec. 1976, pp. 1667-1668.

28. Griffin, M. D.; Anderson, Jr., J. D.; and Diwaker, R.: Navier-Stokes Solutions of the Flowfield in an Internal Combustion Engine. AIAA J., vol. 14, no. 12, Dec. 1976, pp. 1665-1666.

29. Griffin, M. D.; et al.: Computational Fluid Dynamics Applied to the Flow in an Internal Combustion Engine. AIAA Paper No. 78-57, Jan. 1978.

30. Griffin, M. D.; Anderson, Jr., J. D.; and Jones, E.: Computational Fluid Dynamics Applied to Three-Dimensional Nonreacting Inviscid Flows in an Internal Combustion Engine. J. Fluids Eng., vol. 101, no. 3, Sept. 1979, pp. 367-372.

31. Griffin, M. D.: Numerical Solutions for Two- and Three-Dimensional Non-Reacting Flowfields in an Internal Combustion Engine. Ph.D. Thesis, University of Maryland, 1977.

32. Ramos, J. I.; Humphrey, J. A. C.; and Sirignano, W. A.: Numerical Prediction of Axisymmetric Laminar and Turbulent Flows in Motored, Reciprocating Internal Combustion Engines. SAE Paper No. 790356, 1979.

33. Ramos, J. I.; and Sirignano, W. A.: Axisymmetric Flow Model With and Without Swirl in a Piston-Cylinder Arrangement With Idealized Valve Operation. SAE Paper No. 800284, 1980.

34. Ramos, J. I.; and Sirignano, W. A.: Axisymmetric Flow Model in a Piston-Cylinder Arrangement With Detailed Analysis of the Valve Region. SAE Paper No. 800286, 1980.

35. Ramos, J. I.: Axisymmetric Flows in Spark-Ignition Engines. Report CO/80/2, Department of Mechanical Engineering, Carnegie-Mellon University, 1980.

36. Ramos, J. I.; and Sirignano, W. A.: Turbulent Flow Field in Homogeneous-Charge Spark-Ignition Engines. Eighteenth Symposium (International) on Combustion, The Combustion Institute, 1981, pp. 1825-1835.

37. Gosman, A. D.; Johns, R. J. R.; and Watkins, A. P.: Development of Prediction Methods for In-Cylinder Processes in Reciprocating Engines. Combustion Modeling in Reciprocating Engines, J. N. Mattavi and C. A. Amann, eds., Plenum Press, 1980, pp. 69-129.

38. Ahmadi-Befrui, B.; et al.: Multidimensional Calculation of Combustion in an Idealized Homogeneous Charge Engine: A Progress Report. SAE Paper No. 810151, 1981.

39. Boni, A. A.; Chapman, M.; and Schneyer, G. P.: Computer Simulation of Combustion Processes in a Stratified Charge Engine. Acta Astronaut., vol. 3, no. 3-4, 1976, pp. 293-307.

40. Chong, M. S.; Milkins, E. E.; and Watson, H. C.: The Prediction of Heat and Mass Transfer During Compression and Expansion in I.C. Engines. SAE Paper No. 760761, 1976.

41. Matekunas, F. A.: A Schlieren Study of Combustion in a Rapid Compression Machine Simulating the Spark Ignition Engine. Seventeenth Symposium on Combustion (International), The Combustion Institute, 1978, p. 322.

42. Tabaczynski, R. J.; Hoult, D. P.; and Keck, J. C.: High Reynolds Number Flow in a Moving Corner. J. Fluid Mech., vol. 42, no 2, June 1970, pp. 249-255.

43. Daneshyar, H.; Fuller, D. E.; and Deckker, B. E. L.: Vortex Motion Induced by the Piston of an Internal Combustion Engine. Int. J. Mech. Sci., vol. 15, no. 5, 1973, pp. 381-390.

44. Oppenheim, A. K.; et al.: A Cinematographic Study of Combustion in an Enclosure Fitted With a Reciprocating Piston. Paper Presented at the Conference on Stratified Charge Engines, Institute of Mechanical Engineers, London, England, 1976.

45. Ishikawa, N.; and Daily, J. W.: Observation of Flow Characteristics in a Model I.C. Engine Cylinder. SAE Paper 780230, 1978.

46. Bernard, P. S.: Computation of the Turbulent Flow in an Internal Combustion Engine During Compression. J. Fluids Eng., vol. 103, no. 1, Mar. 1981, pp. 75-81.

TABLE I. – GOVERNING EQUATIONS*

Equation	Equation number
$\dfrac{\partial \rho}{\partial t} + \dfrac{1}{r}\dfrac{\partial}{\partial r} r(\rho V_r) + \dfrac{\partial}{\partial z}(\rho V_z) = 0$	1
$\dfrac{\partial}{\partial t}(\rho X_A) + \dfrac{1}{r}\dfrac{\partial}{\partial r} r\left[\rho X_A(V_r + V_{Ar})\right] + \dfrac{\partial}{\partial z}\rho X_A\left[V_z + V_{Az}\right] = 0$	2
$\dfrac{\partial}{\partial t}(\rho V_r) + \dfrac{1}{r}\dfrac{\partial}{\partial r} r\left(\rho V_r^2\right) + \dfrac{\partial}{\partial z}(\rho V_r V_z) = -\dfrac{\partial P}{\partial r} + \dfrac{1}{r}\dfrac{\partial}{\partial r} r\tau_{rr} - \dfrac{\tau_{\theta\theta}}{r} + \dfrac{\partial}{\partial z}\tau_{rz}$	3
$\dfrac{\partial}{\partial t}(\rho V_z) + \dfrac{1}{r}\dfrac{\partial}{\partial r} r(\rho V_r V_z) + \dfrac{\partial}{\partial z}\left(\rho V_z^2\right) = -\dfrac{\partial P}{\partial z} + \dfrac{1}{r}\dfrac{\partial}{\partial r} r\tau_{rz} + \dfrac{\partial}{\partial z}\tau_{zz}$	4
$\dfrac{\partial}{\partial t} e + \dfrac{1}{r}\dfrac{\partial}{\partial r} r\left[(e + P)V_r\right] + \dfrac{\partial}{\partial z}\left[(e + P)V_z\right] = \dfrac{1}{r}\dfrac{\partial}{\partial r} r(\tau_{rr}V_{rz} + \tau_{rz}V_z)$ $+ \dfrac{\partial}{\partial z}(\tau_{rz}V_r + \tau_{zz}V_z) - \dfrac{1}{r}\dfrac{\partial}{\partial r} rq_r - \dfrac{\partial}{\partial z} q_z$	5
$V_{Ar} = -\dfrac{D_{AB}}{X_A}\dfrac{\partial}{\partial r} X_A = -\dfrac{c}{\rho X_A}\dfrac{\partial}{\partial r} X_A$	6
$V_{Az} = -\dfrac{D_{AB}}{X_A}\dfrac{\partial}{\partial z} X_A = -\dfrac{c}{\rho X_A}\dfrac{\partial}{\partial z} X_A$	7
$\tau_{rr} = 2\mu \dfrac{\partial V_r}{\partial r} - \dfrac{2}{3}\mu\left(\nabla \cdot \vec{V}\right)$	8

*C_{pi} = constant pressure specific heat of component i, D_{AB} = binary diffusion coefficient for components A and B, e = energy per unit volume, h_i = specific enthalpy of component i, h_i^0 = standard enthalpy of formation per unit mass for component i at temperature T_i, M_i = molecular weight of component i, P = static pressure, q_j = heat flux in the j-direction, R = universal gas constant, V_j = j-component of the velocity, V_{ij} = j-component of the diffusion velocity for component i, X_i = mass fraction of component i, λ = thermal conductivity, μ = viscosity, ρ = density, τ = shear stress.

TABLE I. – Concluded.

Equation	Equation number
$\tau_{\theta\theta} = 2\mu \dfrac{V_r}{r} - \dfrac{2}{3}\mu\left(\nabla \cdot \vec{V}\right)$	9
$\tau_{zz} = 2\mu \dfrac{\partial V_z}{\partial z} - \dfrac{2}{3}\mu\left(\nabla \cdot \vec{V}\right)$	10
$\tau_{rz} = \mu\left(\dfrac{\partial V_r}{\partial z} + \dfrac{\partial V_z}{\partial r}\right)$	11
$\nabla \cdot \vec{V} = \dfrac{1}{r}\dfrac{\partial}{\partial r}rV_r + \dfrac{\partial V_z}{\partial z}$	12
$X_B = 1 - X_A$	13
$h = X_A h_A + X_B h_B = X_A(h_A - h_B) + h_B$	14
$h_A = h_A^0 + \displaystyle\int_{T_i}^{T} C_{PA}\, dT = h_A^0 + C_{PA}(T - T_i)$	15
$h_B = h_B^0 + \displaystyle\int_{T_i}^{T} C_{PB}\, dT = h_B^0 + C_{PB}(T - T_i)$	16
$q_r = -\lambda \dfrac{\partial T}{\partial r} + \rho X_A V_{Ar}(h_A - h_B) = -\lambda \dfrac{\partial T}{\partial r} - c\left[\left(h_A^0 - h_B^0\right) + (C_{PA} - C_{PB})(T - T_i)\right]\dfrac{\partial}{\partial r}X_A$	17
$q_z = -\lambda \dfrac{\partial T}{\partial z} + \rho V_A V_{Az}(h_A - h_B) = -\lambda \dfrac{\partial T}{\partial z} - c\left[\left(h_A^0 - h_B^0\right) + (C_{PA} - C_{PB})(T - T_i)\right]\dfrac{\partial}{\partial z}X_A$	18
$P = \rho R T\left(\dfrac{X_A}{M_A} + \dfrac{X_B}{M_B}\right) = \rho R T\left[\left(\dfrac{1}{M_A} - \dfrac{1}{M_B}\right)X_A + \dfrac{1}{M_B}\right]$	19

TABLE 2. – BOUNDARY AND INITIAL CONDITIONS

Equation		Equation number
$V_r = 0$, $V_z = u_p$	Piston surface	20
$V_r = V_z = 0$	Cylinder head, cylinder wall, and valve	21
$T = T_v$	Valve	22
$T = T_h$	Cylinder head	23
$T = T_w$	Cylinder wall	24
$T = T_p$	Piston surface	25
$\frac{\partial}{\partial z} X_A = 0$	Cylinder head, valve, and piston surface	26
$\frac{\partial}{\partial r} X_A = 0$	Cylinder wall	27
$P = P_i$, $T = T_i$	Valve opening	28
$X_A = \overline{X}_A + \omega \left(1 - \overline{X}_A\right) \sin\left(\frac{\Omega}{20} t\right)$	Valve opening	29
$X_B = 1 - X_A$	Valve opening	30
$V_r = V_z \tan \alpha$	Valve opening	31
$\frac{\partial \rho}{\partial t} + \frac{1}{r} \frac{\partial}{\partial r} r(\rho V_r) + \frac{\partial}{\partial z}(\rho V_z) = 0$	Valve opening	32
$\frac{\partial \rho}{\partial r} = \frac{\partial X_A}{\partial r} = V_r = \frac{\partial V_z}{\partial r} = \frac{\partial e}{\partial r} = 0$	Center line	33
$\rho = P_c/(RT_i/M_A)$, $X_A = 1$, $V_r = V_z = 0$ $e = P_c \left[(M_A C_{PA} - R)/R + \left(h_A^o - C_{PA}T_i\right)\right]$	$\Big\{$ Everywhere inside the piston-cylinder con- figuration at time $t = 0$	34

TABLE 3. – SUMMARY OF PARAMETERS USED IN THE NUMERICAL CALCULATIONS*

Type of problem	r_p/r_c	Ω(rpm)	P_i/P_c	α(deg)	ω(in eq. (29))	$\overline{X}_A$(in eq. (29))
One-component gas	1.67	400	1	45	0	1
	1.67	400	1.036	0	0	1
	1.67	400	1	0	0	1
	1.67	1000	1	0	0	1
	.78	400	1	0	0	1
Two-component gas mixture	1.67	1000	1	0	1	0.938
	1.67	400	1	0	0	.938
	1.67	400	1	0	1	.938
	.78	400	1	0	1	.938
	1.67	400	1.036	0	1	.938

*The following parameters were the same for all cases studied: $\mu = 3.2 \times 10^{-3}$ kg/m-s, $\lambda = 3.224$ kg-m/s^2-K, $h_A^o = 42,252$ m^2/s^2, $h_B^o = 1.7 \times 10^6$ m^2/s^2, $C_{pA} = 1,006.6$ m^2/s^2-K, $C_{pB} = 1.653.6$ m^2/s^2-K, $M_A = 28.96$ kg/kg-mole, $M_B = 114.2$ kg/kg-mole, $R = 8314.3$ kg-m^2/kg-mole-K-s, $D_{AB} = 3.2 \times 10^{-3}/\rho$ m^2/s^2, $r_p = 0.05$ m, $r_v = 0.01875$ m, $r_H = 0.03438$ m, $\delta(t = 0) = 0.01$ m, $1_c = 0.2$ m, $T_i = T_v = T_h = T_w = T_p = 340$ K, and $P_c = 101,325$ kg/m-s^2.

Results are shown only for the first six cases listed in this table.
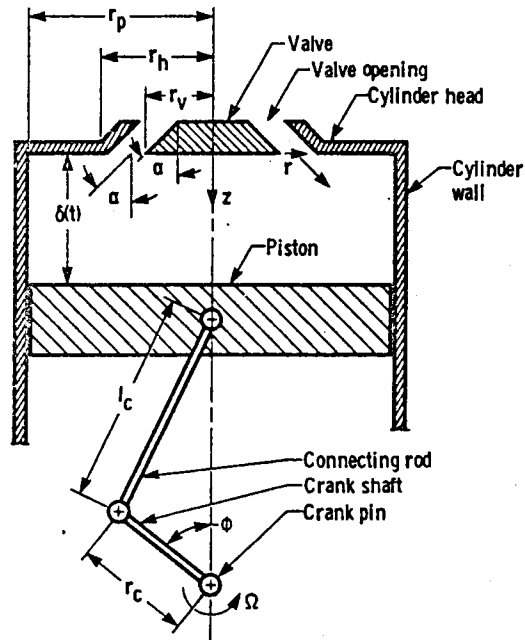
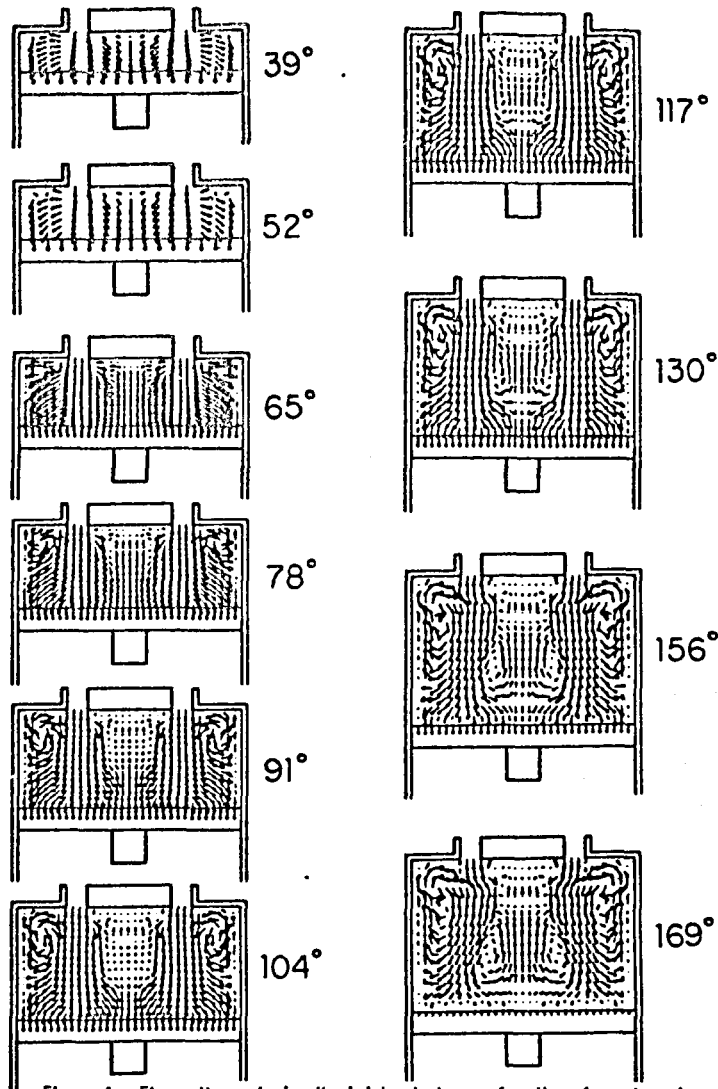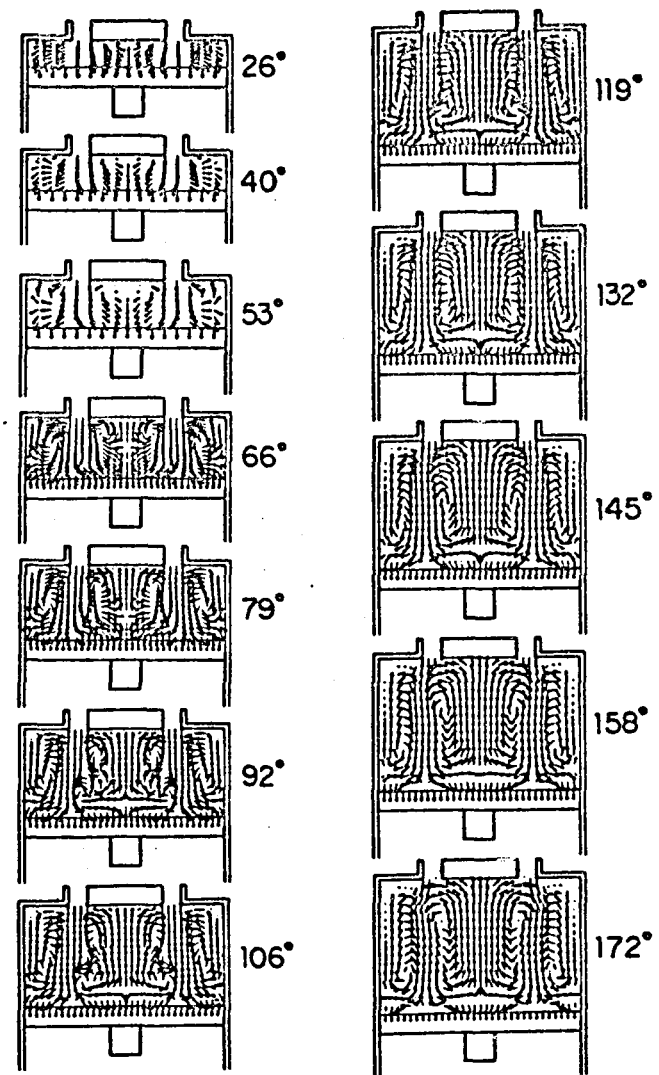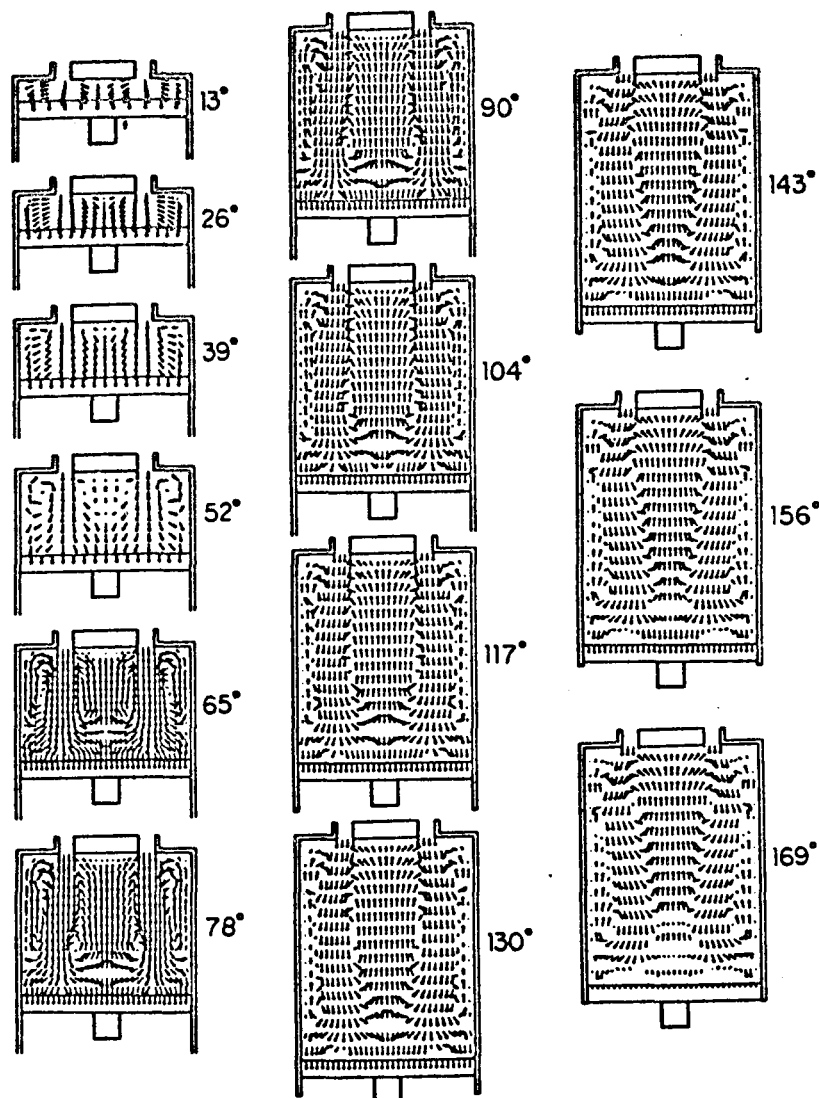Figure 1. - Geometry used in the present study.
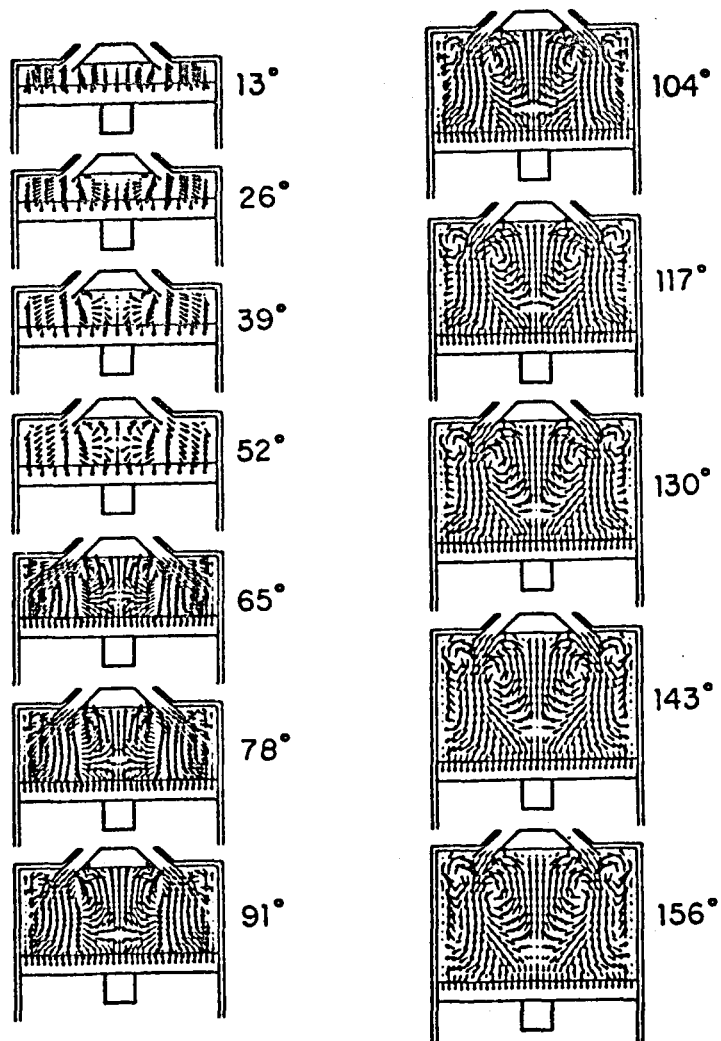
Figure 2. – Flow patterns during the intake stroke as a function of crank angle from TDC for single-component gas, $r_p/r_c = 1.67$, $\Omega = 400$ rpm, $P_f/P_c = 1$, and $\alpha = 45^0$ (Table 3).
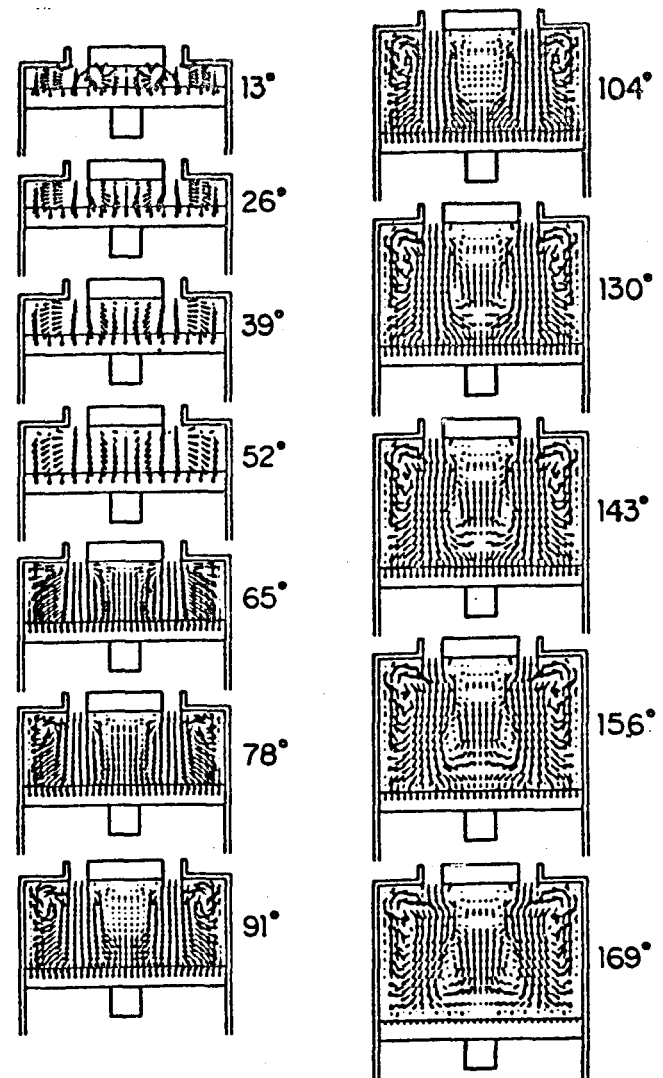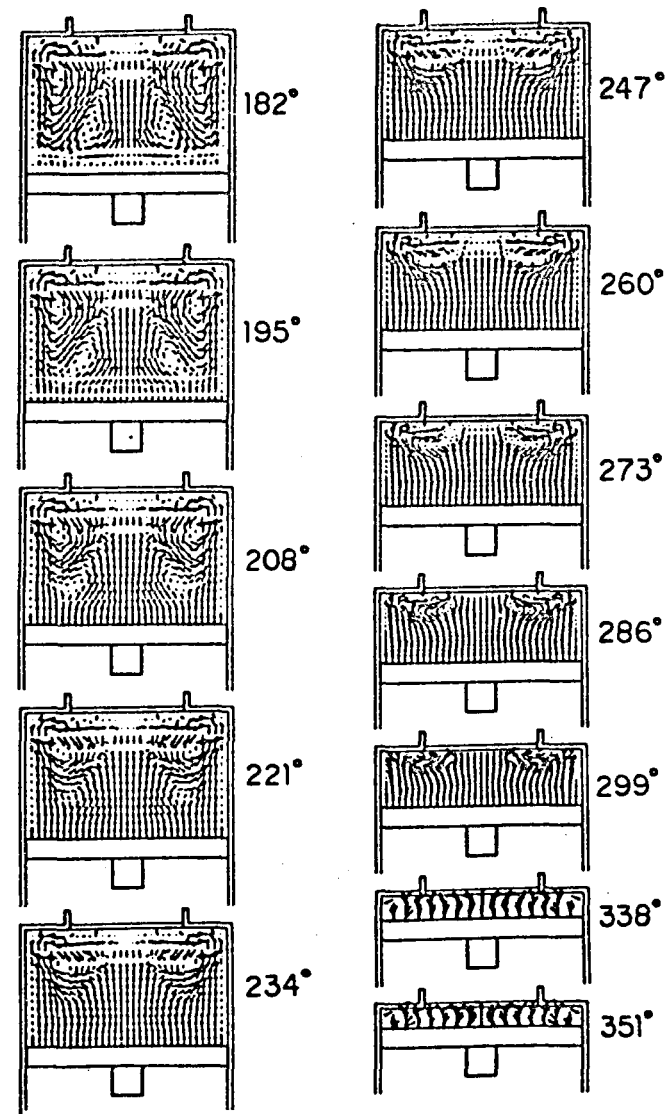

Figure 3. – Flow patterns during the intake stroke as a function of crank angle from TDC for single-component gas, $r_p/r_c = 1.67$, $\Omega = 400$ rpm, $P_f/P_c = 1.036$, and $\alpha = 0^0$ (Table 3).

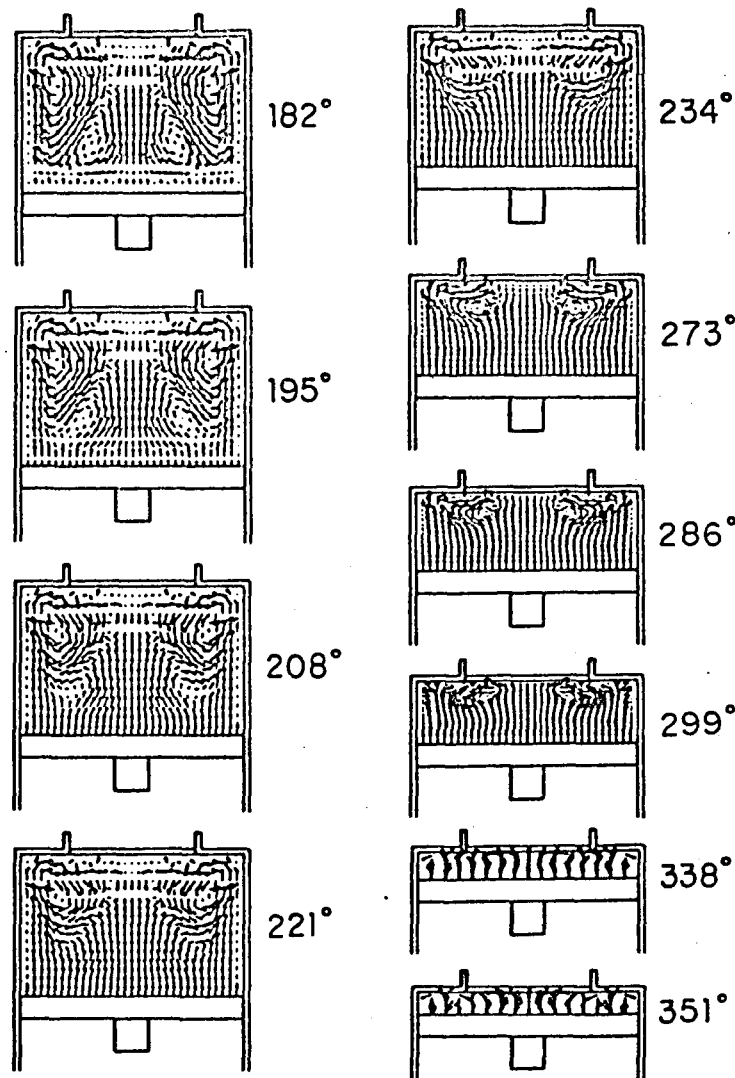Figure 4. – Flow patterns during the intake stroke as a function of crank angle from TDC for single-component gas, $r_p/r_c = 1.67$, $\Omega = 400$ rpm, $P_f/P_c = 1$, and $\alpha = 0°$ (Table 3).

Figure 5. – Flow patterns during the intake stroke as a function of crank angle from TDC for single-component gas, $r_p/r_c = 1.67$, $\Omega = 1000$ rpm, $P_f/P_c = 1$, and $\alpha = 0°$ (Table 3).

Figure 6. - Flow patterns during the intake stroke as a function of crank angle from TDC for single-component gas, $r_p/r_c = 0.78$, $\Omega = 400$ rpm, $P_i/P_c = 1$, and $\alpha = 0^0$ (Table 3).
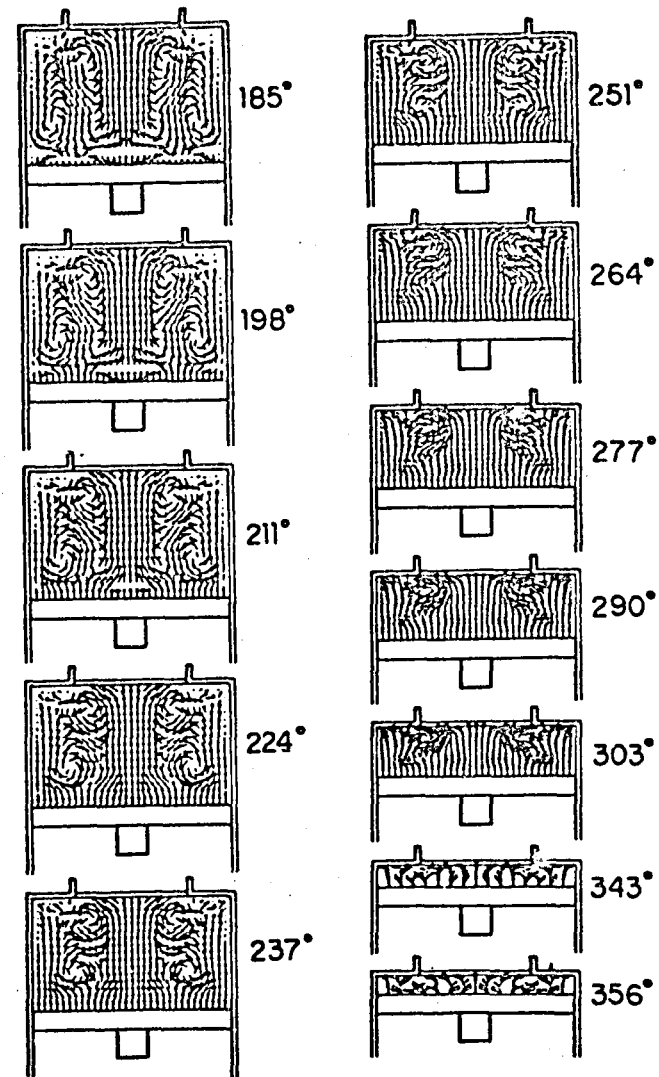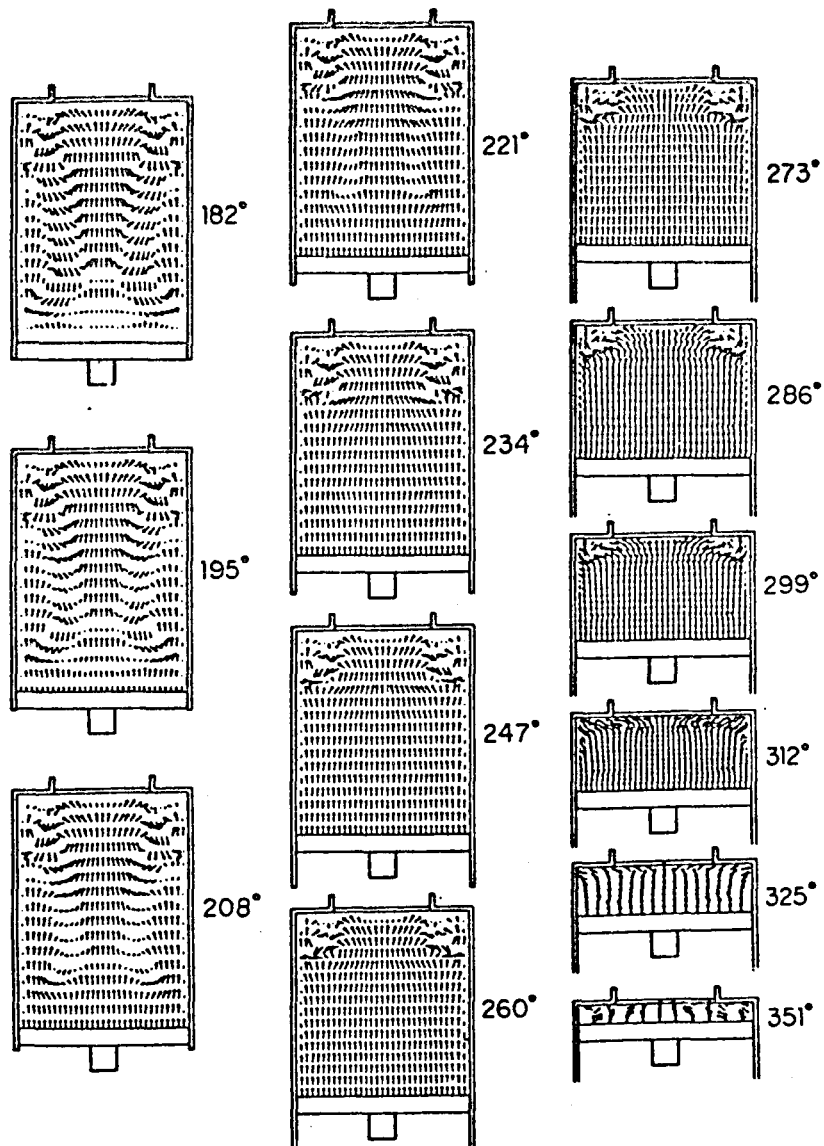

Figure 7. - Flow patterns during the compression stroke as a function of crank angle from TDC for single-component gas, $r_p/r_c = 1.67$, $\Omega = 400$ rpm, $P_i/P_c = 1.036$, and $\alpha = 0^0$ (Table 3).

Figure 8. – Flow patterns during the compression stroke as a function of crank angle from TDC for single-component gas, $r_p/r_c = 1.67$, $\Omega = 400$ rpm, $P_i/P_c = 1$, and $\alpha = 0^0$ (Table 3).

Figure 9. – Flow patterns during the compression stroke as a function of crank angle from TDC for single-component gas, $r_p/r_c = 1.67$, $\Omega = 1000$ rpm, $P_i/P_c = 1$, and $\alpha = 0^0$ (Table 3).

Figure 10. - Flow patterns during the compression stroke as a function of crank angle from TDC for single-component gas, $r_p/r_c = 0.78$, $\Omega = 400$ rpm, $P_i/P_c = 1$, and $\alpha = 0^0$ (Table 3).
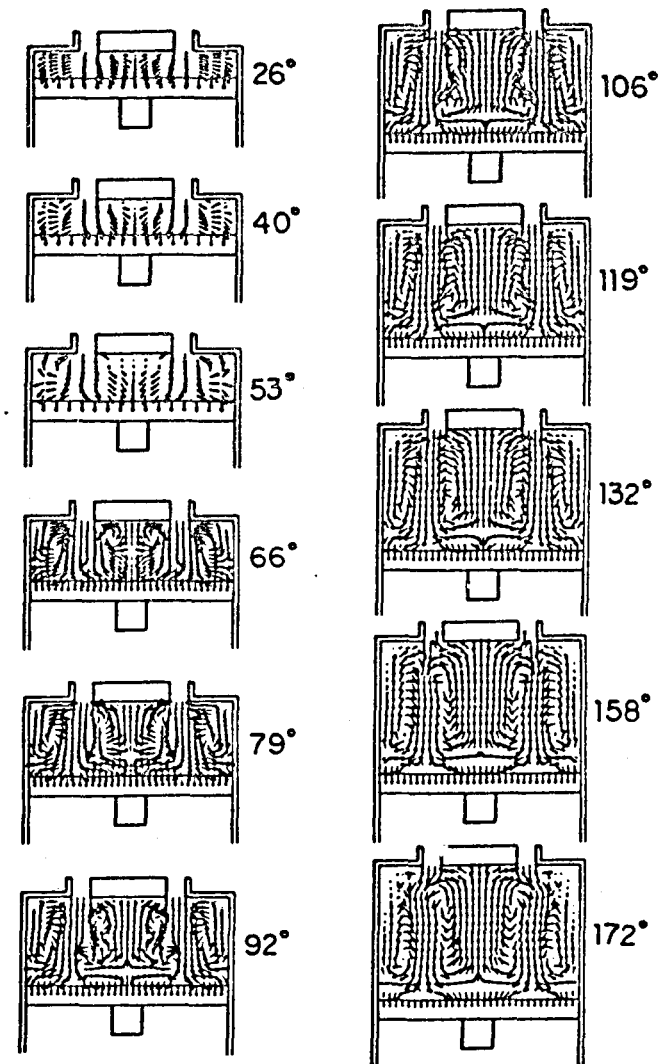

Figure 11. - Flow patterns during the intake stroke as a function of crank angle for two-component gas mixture, $\omega = 1$, $r_p/r_c = 1.67$, $\Omega = 1000$ rpm, $P_i/P_c = 1.0$, and $\alpha = 0^0$ (Table 3).
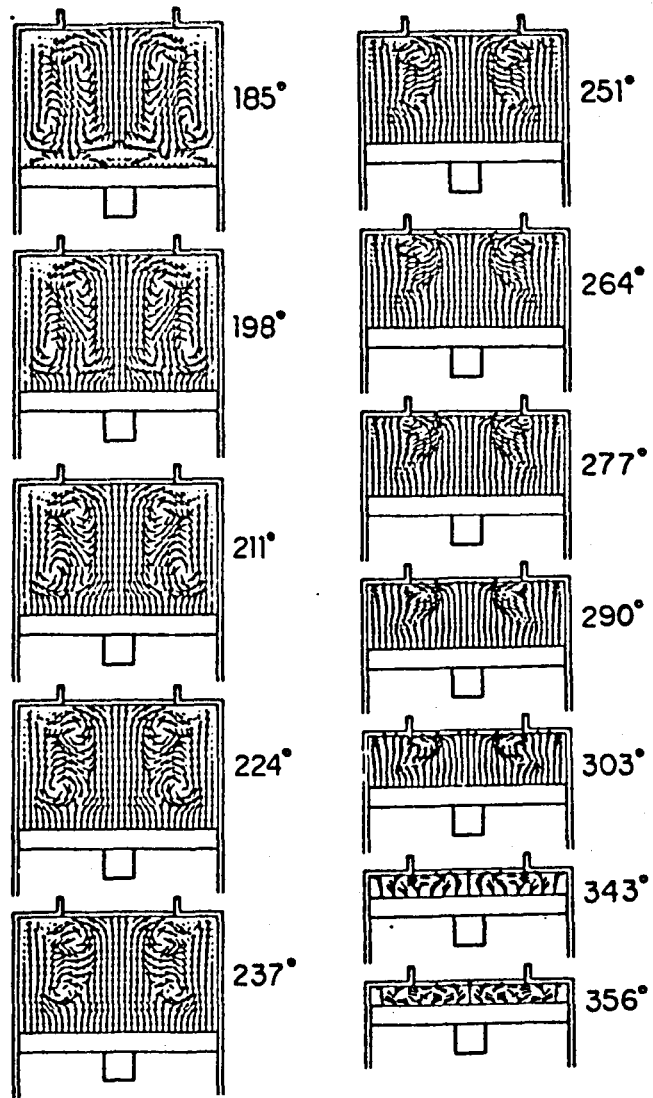
Figure 12. – Flow patterns during the compression stroke as a
function of crank angle for two-component gas mixture, $\omega = 1$,
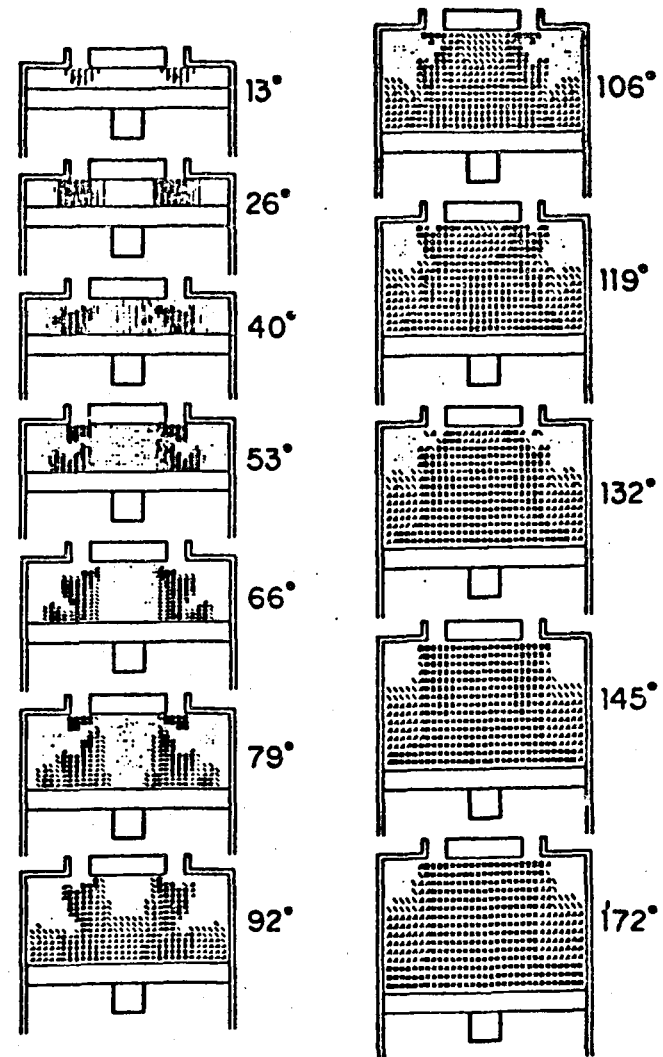$r_p/r_c = 1.67$, $\Omega = 1000$ rpm, $P_I/P_c = 1.0$, and $\alpha = 0^\circ$ (Table 3).

Figure 13. – Distribution of air (component A) to fuel (component B)
ratios during the intake stroke as a function of crank angle from
TDC for two-component gas mixture, $\omega = 1$, $r_p/r_c = 1.67$, $\Omega = 1000$
rpm, $P_I/P_c = 1.0$, and $\alpha = 0^\circ$ (Table 3). Darker regions indicate
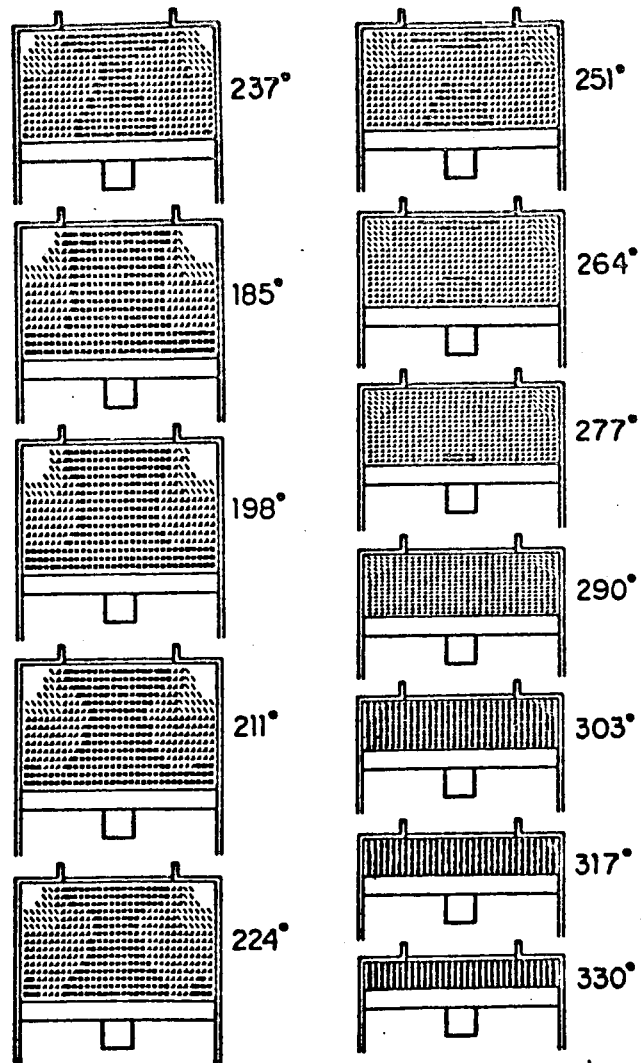lower air-to-fuel ratios.

Figure 14. - Distribution of air (component A) to fuel (component B) ratios during the compression stroke as a function of crank angle from TDC for two-component gas mixture, $\omega = 1$, $r_p/r_c = 1.67$, $\Omega = 1000$ rpm, $P_f/P_c = 1.0$, and $\alpha = 0^0$ (Table 3.) Darker regions indicate lower air-to-fuel ratios.

1. Report No. NASA TM-83011	2. Government Accession No.	3. Recipient's Catalog No.
4. Title and Subtitle NUMERICAL SIMULATION OF THE FLOW AND FUEL-AIR MIXING IN AN AXISYMMETRIC PISTON-CYLINDER ARRANGEMENT		5. Report Date October 1982
		6. Performing Organization Code 505-41-32
7. Author(s) Tom I-P. Shih, Gene E. Smith, and George S. Springer		8. Performing Organization Report No. E-1446
		10. Work Unit No.
9. Performing Organization Name and Address National Aeronautics and Space Administration Lewis Research Center Cleveland, Ohio 44135		11. Contract or Grant No.
		13. Type of Report and Period Covered Technical Memorandum
12. Sponsoring Agency Name and Address National Aeronautics and Space Administration Washington, D.C. 20546		14. Sponsoring Agency Code

15. Supplementary Notes

Tom I-P. Shih, NASA Lewis Research Center; Gene E. Smith and George S. Springer, The University of Michigan, 225 W.E., Dept. of M.E. and A.M., Ann Arbor, Michigan 48109.

16. Abstract

The implicit factored method of Beam and Warming was employed to describe the flow and the fuel-air mixing in an axisymmetric piston-cylinder configuration during the intake and compression strokes. The governing equations were established on the basis of laminar flow. The increased mixing due to turbulence was simulated by appropriately chosen effective transport properties. Calculations were performed for single-component gases and for two-component gas mixtures. The flow field was calculated as functions of time and position for different geometries, piston speeds, intake-charge-to-residual-gas-pressure ratios, and specie mass fractions of the intake charge. Results are presented in graphical form which show the formation, growth, and break-up of those vortices which form during the intake stroke and the mixing of fuel and air throughout the intake and compression strokes. It is shown that at bore-to-stroke ratio of less than unity, the vortices may break-up during the intake stroke. It is also shown that vortices which do not break-up during the intake stroke coalesce during the compression stroke. The results generated were compared to existing numerical solutions and to available experimental data.

17. Key Words (Suggested by Author(s)) Internal combustion engine Fluid mechanics	18. Distribution Statement Unclassified - unlimited STAR Category 34		
19. Security Classif. (of this report) Unclassified	20. Security Classif. (of this page) Unclassified	21. No. of Pages	22. Price*

End of Document